Journal of Structural Geology 32 (2010) 554–565

Contents lists available at ScienceDirect

Journal of Structural Geology

journal homepage: www.elsevier.com/locate/jsg

Role of sedimentation during basin inversion in analogue modelling

Luisa Pinto [a,*], Carolina Muñoz [a], Thierry Nalpas [b], Reynaldo Charrier [a]

[a] Departamento de Geología, FCFM, Universidad de Chile, Plaza Ercilla 803, Casilla 13518, Correo 21, Santiago, Chile
[b] Géosciences Rennes, UMR CNRS 6118-Université de Rennes 1, Campus Beaulieu, 263 Avenue du General Leclerc, 35042 Rennes Cedex, France

ARTICLE INFO

Article history:
Received 8 April 2009
Received in revised form
2 March 2010
Accepted 9 March 2010
Available online 16 March 2010

Keywords:
Basin inversion
Fault reactivation
Syntectonic sedimentation
Shortcuts
Analogue modelling

ABSTRACT

Sand-box experiments were designed to reproduce the effect of sedimentation during extensional basin development and tectonic inversion. These experiments were motivated by growing evidence for tectonic inversion in early Miocene times of an extensional basin (Abanico Basin) in the central Chilean Andes with contemporaneous intense volcanic activity. The experiments perform an extension followed by compression. The first series of experiments were performed without sedimentation in the developing basin; the second series were performed with partial filling of the basin, and the third series with total filling of the extensional basin. The effect of sedimentation on the sides of the basin was also controlled. Compression experiments reproducing tectonic inversion of the previously developed extensional basin were also performed with and without coeval sedimentation (series with null, partial or total fill, and also external sedimentation). The analogue experiments show that high amounts of sediments accumulated during the evolution of an extensional basin enhance subsidence and lead to the development of shortcuts in the footwall of the basin bounding faults during tectonic inversion. During extension the earliest appearance of normal faults occurs in the compartment with the greater sedimentary fill, and this causes asymmetric basin development. The post-extension compressional models show that the greater burden caused by a thicker accumulation of sediments within the basin inhibits tectonic inversion, causing the development of thrust structures rooted in the basin bounding faults. The accumulated sedimentary load affects both the extension and compression phases of the experiments, but has greater influence in the case of sedimentation during extension. A higher burden on the outer edges of the basin compared to the interior enhances the reactivation of normal faults and hampers the development of new thrust structures. The thrust fault(s) originating from the most loaded basin compartment develops as a footwall shortcut from the reactivated fault. With increasing sedimentation the shortcut is developed more superficially. The shortcut absorbs less deformation than the associated main fault.

1. Introduction

The concept of tectonic or structural inversion was generated from the study of petroleum basins (Lamplugh, 1920; Stille, 1924; Pruvost, 1930; Voigt, 1963). Positive tectonic inversion describes those basins that have been initially controlled by extensional faults and later reactivated with a reverse movement during a tectonic compression. Conversely, negative inversion occurs when inverse faults are reactivated with normal movement; however this case is rare (Cooper and Williams, 1989). In this paper, we will refer to positive inversion.

Analogue modelling has been frequently used to understand the mechanisms involved in the tectonic inversion of basins and the origin of associated structures (e.g. Del Ventisette et al., 2005, 2006). This experimental method is a representation of the natural system with materials similar to those existing on the Earth but with a simplified scale. There are several studies that have used analogue modelling to study tectonic inversion. Bally (1984) modeled the inversion process using a hemigraben on a listric fault. He differentiated between partial and total inversion depending on whether there is partial or complete recovery of the pre-graben situation. In the case of total inversion, the reactivation of movement along normal fault(s) results in the recovery of the stratigraphic situation as it was before extension and the extrusion of the basin-fill deposited during extension. The first studies of tectonic inversion used models where a rigid and a mobile block induced the initial geometry of the normal faults (e.g. Bally, 1984; Koopman et al., 1987; McClay, 1989; Buchanan and McClay, 1991, 1992; Mitra, 1993; McClay and White, 1995; Yamada and McClay, 2003a, b). In later models, the experiments were made with free blocks in order to study the geometry and kinematic evolution during extension and compression. Several authors have also analyzed the experimental behavior of several analogue materials

* Corresponding author. Fax: +56 2 6963050.
E-mail address: lpinto@ing.uchile.cl (L. Pinto).

0191-8141/$ – see front matter © 2010 Elsevier Ltd. All rights reserved.
doi:10.1016/j.jsg.2010.03.001

including sand, clay and silicone (Richard and Cobbold, 1990; Nalpas and Brun, 1993; Nalpas et al., 1995; Brun and Nalpas, 1996; Keep and McClay, 1997; Dubois et al., 2002; Panien et al., 2005). Furthermore, it has been also shown that to produce inversion along high-angle normal structures in a brittle system modeled by analogue experiments, a non-coaxial angle between the compressive and extensive stresses is required (Brun and Nalpas, 1996; Gartrell et al., 2005), with an optimum angle for inversion close to 15° (Brun and Nalpas, 1996). Other studies have shown that inversion can be generated with higher angles even with orthogonal compression (Del Ventisette et al., 2006). However, these systems have been modeled generally with large ductile silicone basal layers, which creates an experimental device more easily deformable that even produces rotation of blocks on the dip direction of the faults (Brun et al., 1994; Corti et al., 2003; Del Ventisette et al., 2006). An interesting geometry generated in inverted systems results from the development of new thrust faults in the footwall block, named "footwall shortcuts", that absorb further deformation in the inverted systems (Buchanan and McClay, 1991, 1992); but there is little analysis of their evolution and the specific factors that influence it.

There are abundant worldwide examples of regions where extension has been followed by tectonic inversion. There are classic cases of inversion in marine environments in North America, and other mountain chains (e.g. Hansen, 1986; Stone, 1989; Walker and Cooper, 1986; Buchanan and Buchanan, 1995; Knott et al., 1995; Lowell, 1995). In the Andean subduction margin, there are good examples of extensional basins, i.e., the Jurassic and Early Cretaceous back arc basins, and the Late Cretaceous and Paleogene intra-arc basins, which underwent tectonic inversion (e.g. Jordan et al., 2001; Charrier et al., 2002, 2007). Inversion, in these cases, occurred during major changes of plate dynamics that resulted in modification of the stress regime affecting the continental margin (e.g. Pardo-Casas and Molnar, 1987). A well studied case is the Abanico Basin (e.g. Vergara and Drake, 1979; Nyström et al., 1993, 2003; Kay and Kurtz, 1995; Charrier et al., 2002; Muñoz et al., 2006), developed between Middle Eocene and Late Oligocene times in the Principal Cordillera of central Chile (e.g. Charrier et al., 1994, 2002, 2005; Godoy and Lara, 1994; Burns and Jordan, 1999; Godoy et al., 1999; Jordan et al., 2001; Fock 2005; Fock et al., 2006a, b). In this basin, thick deposits of lava, volcaniclastics and minor sediments were accumulated during extension. Deposition was uninterrupted by the start of the inversion, and continued to form a new and thick volcanic succession (e.g. Charrier et al., 2002, 2005, 2007; Fock 2005; Fock et al., 2006a, b). Therefore, it is particularly interesting to understand how a partial inversion of the basin was possible along with the coeval accumulation of thick volcanic successions. Moreover, the volcanic rocks accumulated during tectonic inversion host giant Late Miocene porphyry Cu–Mo deposits such as Los Pelambres, Río Blanco-Los Bronces and El Teniente, which were emplaced along fault systems associated with the extension and tectonic inversion of the Abanico Basin (Garrido et al., 1994, 2002; Rivera and Cembrano, 2000; Rivera and Falcón, 2000; Charrier et al., 2002, 2005; Godoy, 2005). Deposition coeval to tectonic inversion (i.e. volcanic activity during compression) has not yet been considered by analogue models. In terms of mass transfer, this situation does not correspond to the classic definition of inversion (Voigt, 1963). Some analogue modelling experiments have attempted to assess the influence of sedimentation on basin development, depositing material in the basin at later stages in the extension and pre-compression phases (Nalpas and Brun, 1993; Nalpas et al., 1995; Brun and Nalpas, 1996; Dubois et al., 2002; Panien et al., 2005). These studies show that if there is no sedimentation all normal faults are reactivated to some extent, whereas with sedimentation the reactivation of the structures is limited, generating thrusts and backthrusts that cut and accommodate shortening (Dubois et al., 2002; Panien et al., 2005). However, so far no systematic attempt has been made to evaluate the influence of sedimentation on extensional basin development or the evolution of basin inversion considering all possible cases of syntectonic sedimentation. The inversion associated with deposition of volcanic deposits, and the fact that there are no detailed studies on the subject, has motivated the development of analogue models experiments described here. The application of the results to the Abanico Basin will be the focus of a future publication.

The aim of this study is to understand the effect of syntectonic sedimentation on basin development during inversion, by the way of analogue modelling. The key parameter is the location and amount of sedimentation during both extension and compression. The experiments are designed in order to simulate not only the geological example presented (from the Andean system), but also to simulate the general situation of inverted basins.

2. Analogue modelling

Modelling techniques used in these experiments are similar to those used in the experiments of brittle–ductile systems at the Laboratory of Experimental Tectonics of the Department of Geosciences, Université de Rennes I, described in detail in the literature (e.g. Faugère and Brun, 1984; Vendeville et al., 1987; Davy and Cobbold, 1991). Brittle behavior is represented by sand, with a mean friction coefficient (φ) of 0.58, a density (ρ) of 1400 kg/m^3 and a medium sand average grain size between 297 and 425 μm. Ductile behavior is represented by a mass of transparent silicone with a viscosity (μ) of 4×10^4 Pa/s at 20 °C and a density (ρ) of 960 kg/m^3 (Davy and Cobbold, 1991). The scaling parameters for extension and compression are included in Table 1.

The experimental device is similar to the one often used to model grabens and graben inversion in analogue experiments (Allemand et al., 1989; Allemand and Brun, 1991; Tron and Brun, 1991; Brun and Nalpas, 1996). It consists of a fixed and rigid base, on which a thin plate moving at a constant rate is pulled (extension) or pressed (compression) (Fig. 1). The limit of the mobile plate induces an asymmetric velocity discontinuity (VD) in the base of the model (Malavielle, 1984; Balé, 1986; Allemand et al., 1989; Ballard, 1989). The angle of obliquity used in the compressive experiments is 30° with respect to the VD (Fig. 1a) and is the best angle to produce inversion in analogue experiments according to previous studies (Letouzey, 1990; Brun and Nalpas, 1996; Panien et al., 2005; Del Ventisette et al., 2006). However, it should be noted that there are other parameters in nature that facilitate inversion, which in the aim of simplicity have not been considered here, such as the presence of internal fluids and/or ductile minerals along the fault-plane. For this reason, inversion in the presence of such factors might be produced with greater angles. Therefore, the results obtained from our experiments are not only applicable to oblique tectonic regimes, but also to more orthogonal compressive systems.

The models were built primarily with sand to represent the basement and brittle cover. In addition, a fine layer of silicone was added (1 cm thick) on top of the VD to distribute the strain on it and create a wider zone of deformation. In these experiments the silicone does not simulate any character of the crust and has exclusively a geometrical use (Brun and Nalpas, 1996). The dimensions of the experimental device are shown in Fig. 1. The basal plate used to generate the VD is glued to the mobile wall and is 0.5 mm thick and 22 cm long. The dimensions of the silicone layer are 5 cm wide, 1 cm thick and 60 cm long. Over the silicone a 5 cm thick layer of sand was placed (Fig. 1a).

Two groups of experiments were performed during this study. The first group consisted of models with extension orthogonal to the

Table 1
Definition of fixed parameters used in the experiments.

General parameters of experiments						
	Angle with respect to VD			Velocity (cm/h)	Time (min)	Quantity (cm)
Extension	90°			2	45	1.5
Compression	30° dextral			2	90	1.5
Parameters of scaling						
	L (m)	g (m/s^2)	ρ (kg/m^3)	μ (Pa/s)	V (m/s)	t (s)
Nature	3000 (3 km)	9.81	2700	6×10^{20}	6.3×10^{-11} (0.2 cm/y)	9.5×10^{13} (3 My)
Model	0.01 (1 cm)	9.81	1400	4×104	5.5×10^{-6} (2 cm/h)	3.7×10^{3} (1 h)
Model/nature ratio	3.3×10^{-6}	1	0.52	6.7×10^{-17}	8.6×10^{4}	3.9×10^{-11}

Particular experimental conditions for each model carried out							
Experimental run	Code[a]	Sedimentation during extension			Sedimentation during compression		
		Processes involved	Internal and partial	Internal and complete	Internal and partial	Internal and complete	External
ITACES 23	a	e	–	–	–	–	–
ITACES 15	b	e	x	–	–	–	–
ITACES 7	c	e	–	x	-	–	–
ITACES 6	d	e–c	–	–	-	–	–
ITACES 11	e	e–c	x	–	-	–	–
ITACES 8	f	e–c	–	x	-	–	–
ITACES 22	g	e–c	–	–	x	–	–
ITACES 12	h	e–c	x	–	x	–	–
ITACES 14	i	e–c	–	–	–	x	–
ITACES 10	j	e–c	–	x	–	-	x
ITACES 20	k	e–c	–	–	–	x	x
ITACES 21	l	e–c	x	–	–	x	x
ITACES 9	m	e–c	–	x	–	x	x

VD, velocity discontinuity; L, length; g, gravity; ρ, density; μ, viscosity; V, Velocity; t, time; e, experiment someted to extension; c, experiment someted to compression.
[a] Code refers to the correspondent experiment shown in Figs. 2 and 5.

VD to create a basin parallel to it. In the second set an oblique compression after the extension was applied over the sandboxes, with an amount of 'orthogonal shortening' equal to the previously obtained extension (1.5 cm), to promote the maximum reactivation of normal faults to reverse (Fig. 1). To obtain this orthogonal shortening we applied an angle of 30° of the mobile wall with respect to the VD and to the basin (Fig. 1b). The orthogonal shortening was calculated from a projection of the compressive movement vector on the perpendicular line to the mobile wall (Fig. 1). For simplicity in this paper 'shortening' refers to 'orthogonal shortening'. In all experiments the parameters used to define the extension and compression remained fixed and are summarized in Table 1.

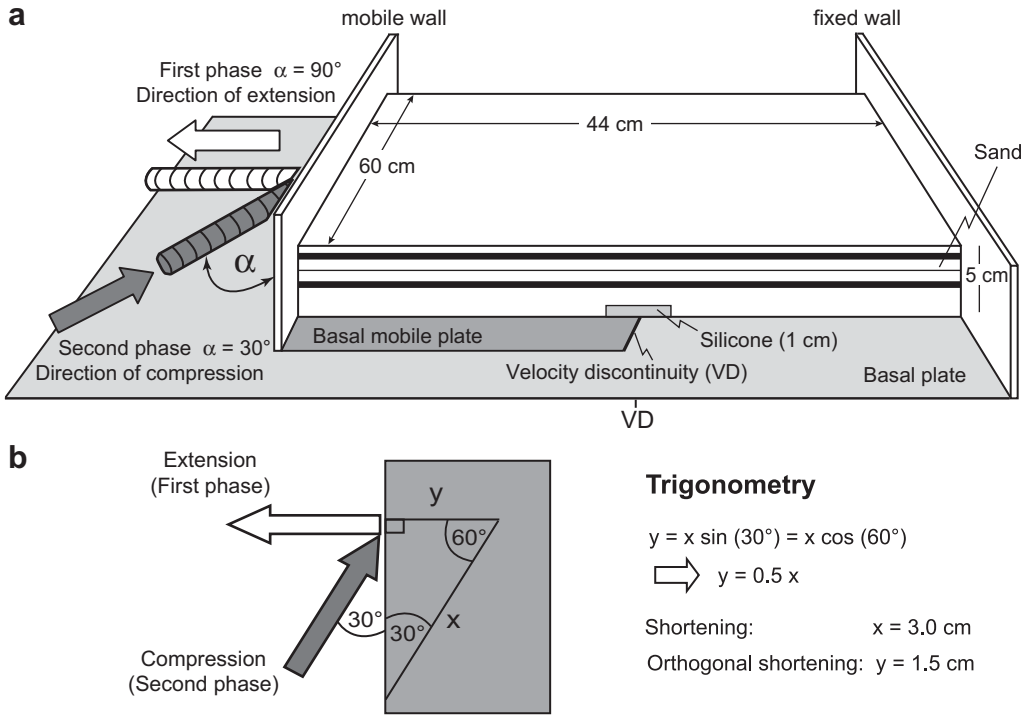

Fig. 1. (a) Sketch of the experimental device, assembly and fixed dimensions for all models. The angle used during the extensional and compressive phase, 'α', is indicated. (b) Sketch of top-view model showing the relation between the slide in the compressive direction ('x') and the shortening orthogonal to VD ('y').

We note that 100% extension was reached after 45 min (a total of 1.5 cm lengthening), and on this basis we estimated the temporary development of the structures. In compression, 100% of shortening was reached after 90 min (a total of 1.5 cm orthogonal shortening) starting immediately after the extension. In both types of models, the contemporary sedimentation was made by continuously adding thin layers of alternating colors of sand at different rates depending on the analyzed model in and/or outside the basin. The deposition was hand-made with a sieve, therefore we did not have high precision on the deposition thickness or rate of sedimentation; the quantity of deposition depended on the accumulation space for each case. For both groups of models only the most likely combinations observed in nature were carried out. For the extensional series, three models were made (Fig. 2a–c): (1) Without sedimentation, (2) with partial sedimentation and (3) with complete sedimentation or complete filling of the developed basin (Table 2). The compressive models were based on the same extensional series, and we developed three compressive series (Fig. 2d–m): (1) without sedimentation, (2) with partial sedimentation and (3) with complete sedimentation (Table 3). Experiments with complete sedimentation in extension, and complete or partial sedimentation in compression, were not carried out as this is a situation that does not exist in nature; the basin is infilled and had no more accommodation space. Similarly, the models with partial sedimentation in extension and in compression were not made because of technical difficulties recreating them.

The analysis of the development of structures on the surface was hampered by sedimentation in various cases. Top-view photographs were taken at regular intervals to study the time–space evolution of the structures (Tables 2 and 3). The time of occurrence of faults was measured during the experiments by simple observation of the surface of the model, and therefore this time does not represent the real commencement of structure formation as they could have started earlier and deeper than recorded. Despite this, we could determine their progressive evolution with the observed timings. The analysis of the final internal deformation of the experiments was performed by cutting profiles at the center of the model, perpendicular to the VD, in order to obtain a more general view of the region least affected by edge conditions associated with the experimental device. The timing of fault development and reactivation was determined on the basis of cross-cutting relations of the faults.

3. Results

3.1. The extensional phase

The main deformation generated in the extensional phase comprised four parallel faults, forming two parallel grabens organised in a subsidence zone or “basin” along the VD (Figs. 2a–c and 3), sediments were accumulated in these grabens. These grabens, G1 and G2, each one defined by two conjugate normal faults: G1 was defined by N1 and n1, and G2 was defined by n2 and N2 (Fig. 3). The properties of both the faults (angle, time of onset and amount of extension) and the basin defined by them (depth, width, subsidence area) are presented in Table 2. The width of the generated basin was similar in all experiments, with an average of 11.3 cm (Fig. 4c and Table 2), but the depth of basin is different in each model and depends on the amount of sedimentation (see below). All the developed faults were high-angle, varying in dip from 62° to 76°. The fault surfaces are approximately planar with only slight curvatures and/or branches (Fig. 5a–c). There are different points of nucleation for normal faults, however this is random and does not bear relation to the sedimentation (Fig. 5a–c).

In all experiments the order of appearance of the normal fault was as follows: N1, N2, n1 and n2 (N1 and N2, being the faults bounding the grabens externally, and n1 and n2, being the faults bounding the grabens internally) (Figs. 2a–c, 3 and 5a–c, and Table 2). However, as sedimentation increased, the second appearance of the external normal fault (N2) was gradually delayed (Fig. 4a and Table 2), for example without sedimentation fault N2 appeared when the extension was at 24.4% (11 min/45 min), whereas in the case of complete sedimentation this fault appeared when the extension was at 33.3% (15 min/45 min). In contrast, the emergence of internal faults (n1 and n2) was gradually advanced (Fig. 4a and Table 2), for example in the case without sedimentation fault n1 appeared with a 55% (25 min) of extension, while in the case of complete sedimentation it appeared when the extension was 33% (15 min/45 min). In models where sedimentation was partial and complete, sedimentation began in the escarpment N1. This can be clearly displayed, representing the time of formation of grabens by the difference of time between the formation of faults N1 and n1 and faults n2 and N2, which became progressively smaller (Fig. 4b).

In general, the external normal faults, N1 and N2, developed a lower dip angle (62°–67°) than the internal ones, n1 and n2 (63°–76°) (Table 3 and Fig. 4f). With this lower angle, N1 and N2 accommodated most of the extensional deformation, measured as horizontal displacement (Fig. 5a–c). On the other hand, the normal internal faults, n1 and n2, primarily accommodated the vertical movement with a smaller horizontal displacement because of their higher angle (Fig. 5a–c).

Increasing the sediment load (from without sedimentation, to partial sedimentation and then complete sedimentation) increases the depocenter depth of the basin (Figs. 4d and 5a–c), from 0.8 cm in the case without sedimentation to 1.4 cm in the case of complete sedimentation. Therefore, because G1 was generally the first graben to be formed the increasing sedimentary load meant that this graben was progressively deeper (Fig. 4e), and consequently the faults N1 and n1 developed more movement than faults N2 and n2. The later faults showed a slight decrease in vertical throw in the experiments with increased sedimentation. The increase of deformation in one major graben (G1) related to sedimentation favored the decrease of movement in the minor graben (G2) and its delay in formation time.

3.2. The shortening phase

For this series of experiments, the extensional basin had the same size and configuration as in previous reference experiments depending on the sediment load (see Section 3.1). The main structures obtained during the shortening phase, compression after extension, are the reactivated older normal faults (R1, R2, r1, r2) and the creation of two new thrust faults (I1 and I2) of low angle and located on the outer edges of the inverted grabens (Figs. 2d–m, 5d–m and 6). In some experiments, a new thrust fault within the grabens was generated (i1, Figs. 5d, e, h and 6). In addition, dextral strike-slip faults approximately parallel to the compressive direction were formed on the border of the sandbox related to boundary conditions (Fig. 6). The geometric and temporal characters (time of onset, angle and horizontal shortening) of the structures generated during the compression, both the ones seen on the surface and those seen in sections, are summarized in Table 3. In addition, the newly formed thrust faults show a slight curve in their superficial trace (Fig. 5d–m).

To determine the amount of tectonic inversion associated with each experiment, we calculated a percentage of inversion (Table 3). This amount of inversion is associated with shortening orthogonal to the VD and refers to reverse fault reactivation in the previously formed normal faults (Fig. 1b). The amount of reactivation in the

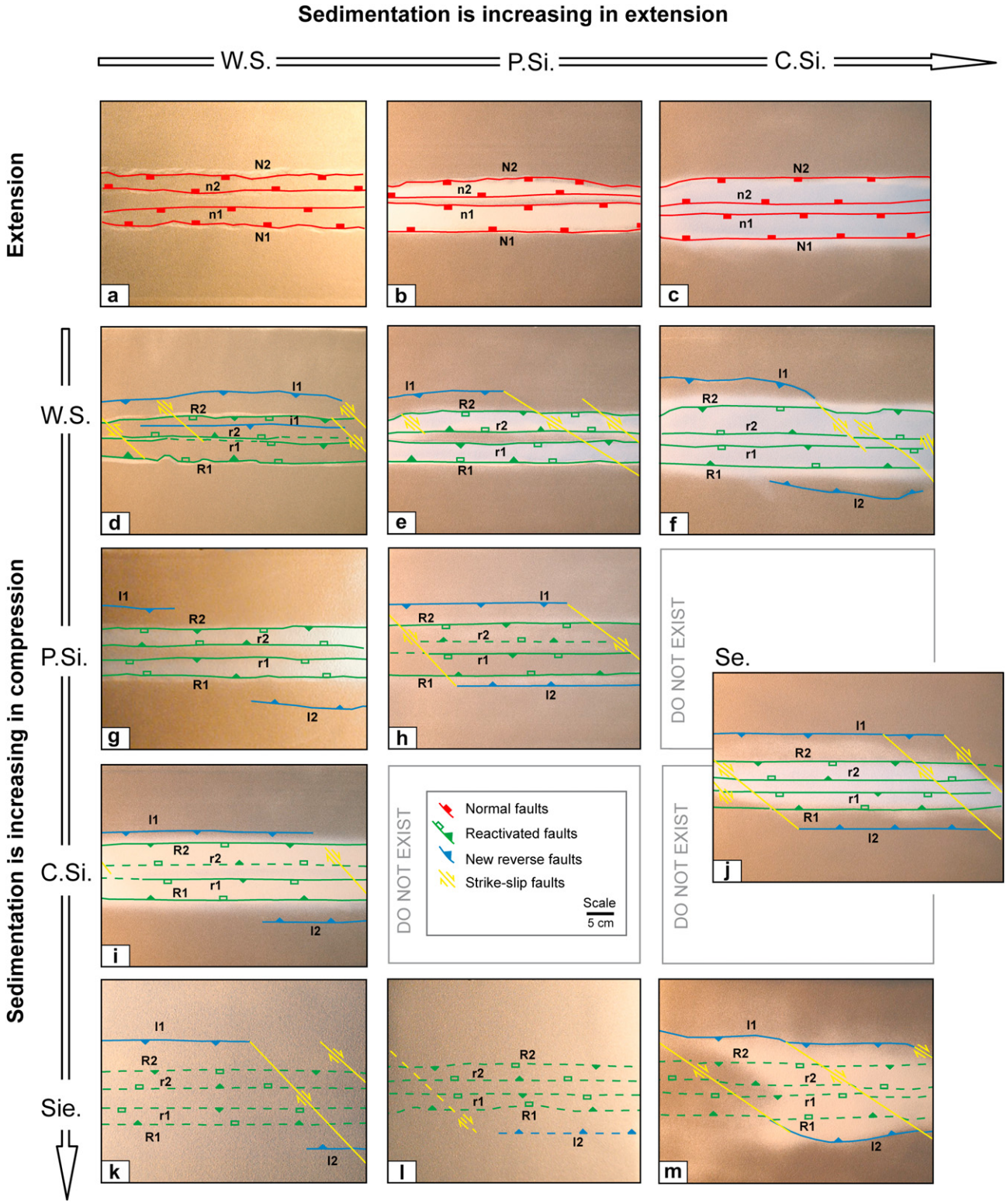

Fig. 2. Photographic summary of top-view final state of experiments in extension and compression. Legend: Lines with filled boxes (red lines in digital version) indicate normal faults developed during extension (N1, N2, n1 and n2); lines with empty boxes and filled triangles (green in digital version) indicate reactivated normal faults (R1, R2, r1 and r2); lines with filled triangles (blue in digital version) indicate the new reverse faults (I1, I2, i1); lines with arrows on both sides (yellow in digital version) are strike-slip faults produced by boundary conditions associated with the experimental device. The numbers '1' and '2' indicates the order of occurrence for each kind of faults. Segmented lines indicate inferred faults. Label of experiments is the same used in Fig. 5 and in the tables. Abbreviations: W.S., without sedimentation; P.Si., partial internal sedimentation; C.Si., complete internal sedimentation; Sie., internal and external sedimentation; Se., external sedimentation. (For interpretation of the references to colour in this figure legend, the reader is referred to the web version of this article).

Table 2
Results of extensional experiments. The timing of structures is based on a total time of 45 min with a total experimental lengthening of 1.5 cm.

	Faults	Characteristics	Ext. without sedim. (ITACES 23) – a*	Ext. with partial sedim. (ITACES 15) – b	Ext. with complete sedim. (ITACES 7) – c
Normal faults	N1	Toc (min)	10	10	10
		Angle (°)	67	64	63
		QExt (mm)	4.0	4.5	6.5
	n1	Toc (min)	25	20	15
		Angle (°)	68	63	76
		QExt (mm)	3.0	2.5	3.5
	N2	Toc (min)	11	13	15
		Angle (°)	66	63	62
		QExt (mm)	5.5	6.0	3.5
	n2	Toc (min)	27	23	20
		Angle (°)	71	73	68
		QExt (mm)	2.5	2.0	1.5
Grabens and Basin	G1	Width (cm)	5.5	5.6	4.7
		Depth (cm)	0.5	0.8	1.4
	G2	Width (cm)	5.0	4.9	5.1
		Depth (cm)	0.80	0.95	0.50
		Grabens distance (cm)	1.5	0.5	1.2
	Basin	Overall width (cm)	12	11	11
		Max. depth (cm)	0.80	0.95	1.4
		Ratio (depth/width)	0.067	0.086	0.127
		Subsidence area	7.90	7.76	7.70

Ext., extension; Sedim., sedimentation; Toc, time of occurrence; QExt, amount of extension absorbed by the fault; N,n, normal faults; G, Grabens; 1, 2, order of occurrence.
*'ITACES' refers to experimental run and letters a, b and c refer to the correspondent experiment in Figs. 2 and 5.

strike component could be measured directly in the top-view of the experiments. However, we could not determine clearly the reverse reactivation, since we had no marker for it. Therefore, the estimated proportion of inversion is calculated indirectly considering our knowledge of the total amount of compression orthogonal to the VD, equal to 1.5 cm, and quantity of shortening of the new reverse faults (Fig. 1b). Thus, reactivation would equal the total amount of orthogonal shortening minus the amount absorbed by the new reverse faults. Then the percentage of inversion would be represented as follows:

$$\%\ \text{Inversion} = \frac{100 \times \text{Applied orthogonal shortening} - \text{Orthogonal shortening associated to reverse structures}}{\text{Applied orthogonal shortening}} \quad (1)$$

The shortening associated with the reverse structures was measured directly on the profiles perpendicular to the mobile wall, where we could see displacement over these structures. In the case of curved faults, the largest shortening was measured in the

Table 3
Results of compressive experiments. The timing of structures is based on a total time of 90 min with a total experimental shortening of 1.5 cm (orthogonal to the VD).

Structures	Experiment	Ext. without sedim. (ITACES 6)[a]	Ext. with partial sedim. (ITACES 11)	Ext. with complete sedim. (ITACES 8)	Ext. without sedim. (ITACES 22)	Ext. with partial sedim. (ITACES 12)	Ext. without sedim. (ITACES 14)	Ext. with complete sedim. (ITACES 10)	Ext. without sedim. (ITACES 20)	Ext. with partial sedim. (ITACES 21)	Ext. with complete sedim. (ITACES 9)
		Compression without sedimentation			Compression with partial sedimentation		Compr. with complete sedim.	Compr. with external sedim.	Compression with internal and external sedimentation		
		d[b]	e	f	g	h	i	j	k	l	m
I1	Toc (min)	60	75	45	70	70	70	50	75	–	50
	Angle(°)	40	39	34	37	40	39	36	30–50[c]	25–50[c]	42
	Short. (mm)	2.0	3.0	7.0	3.5	2.0	1.5	4.0	4.0	5.0	6.0
i1	Toc (min)	70	–	–	–	–	–	–	–	–	–
	Angle (°)	45	40	–	–	40	–	–	–	–	–
	Short. (mm)	1.0	1.0	–	–	0.5	–	–	–	–	–
I2	Toc (min)	–	80	50	70	70	75	50	75	–	50
	Angle (°)	–	40	40	35–40[c]	40	41	40	30–50[c]	25–50[c]	43
	Short. (mm)	–	4.0	1.0	3.5	2.0	3.0	3.0	4.0	5.0	1.0
SSF	Toc (min)	45	60	30	20	60	65	20	45	–	20
Highest point (mm)		2.0	3.0	6.5	5.0	2.0	2.5	4.0	2.0	3.5	5.0
Inversion percentage (%)		80	73	47	77	70	70	53	73	67	53

Ext., extension; Sedim., sedimentation; Compr., Compression; I,i, New Reverse Faults; 1,2, order of occurrence; Toc, time of occurrence; QExt, amount of extension absorbed by the fault; N,n, normal faults; G, Grabens; 1, 2, order of occurrence.
[a] 'ITACES' refers to experimental run.
[b] We show the associated letter of the experiment in Figs. 2 and 5.
[c] Faults are courved and its dip is variable.

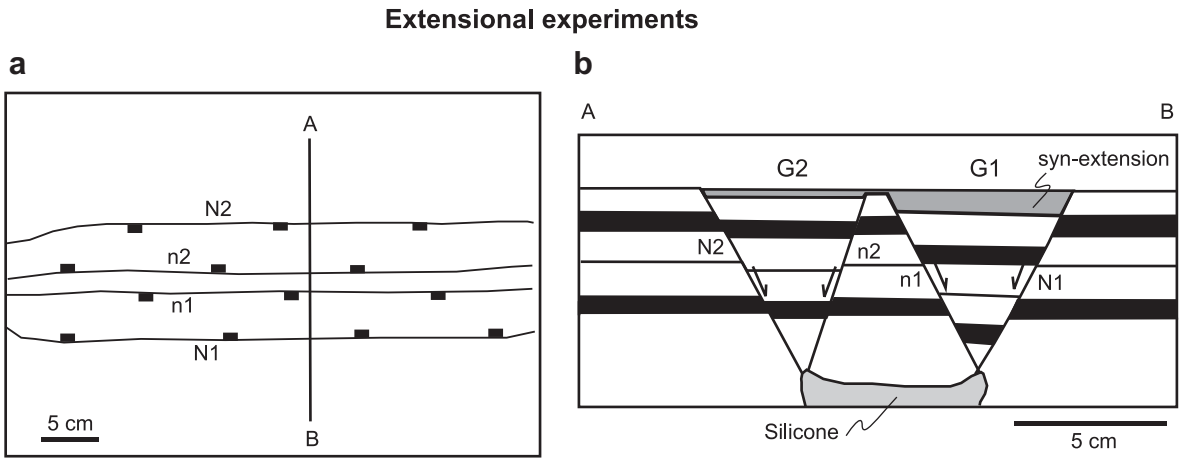

Fig. 3. Schematic illustration of the final state of the main structures formed in the extension experiments, showing the extreme case as an example. (a) View from above of the experiment. The boxes indicate the dip direction of the normal faults. The labeling of faults is as follow: N, n, normal fault; G, Graben; 1 and 2, order of occurrence. (b) Section A–B through the central part of the experiment, where 'A' corresponds to the mobile wall side (where the piston is located) and 'B' to the fixed wall side. Arrows indicate the movement direction of the normal faults. The syn-extensional area shows the possible place for the sedimentary filling.

horizontal direction, associated with the smaller angle. It can be seen in several models that some previous faults are not reactivated inversely, but we assume that part of the total orthogonal shortening must be absorbed by normal faults reactivated in reverse since not all the shortening is absorbed into the new reverse faults (Table 3). Moreover, it is probable that the amount of inversion is slightly overestimated because we do not consider the compaction of the sand. However, given the same compression settings and the same materials, the compaction should be the same for all experiments and, therefore, should not be significantly different allowing comparison between models.

The compressive experiments showed that the beginning of the inversion of the normal faults (R1, r1), was delayed by the amount of sediment previously accumulated in the grabens (Fig. 4g). For example, in the case of extension and compression without sedimentation, these faults were reactivated when shortening was 17% (15 min/90 min), whereas in the case of extension with partial sedimentation followed by a compression without sedimentation, reactivation of the faults started at 33% shortening (30 min/90 min) (Fig. 4g).

In nearly all the models two new reverse faults were formed (I1 and I2) (Figs. 2 and 5d–m). For these faults dip-slip as well as strike-slip occurred. In some of the presented sections these faults do not appear coevally, because they were not developed enough (e.g. Fig. 5e, g, k and l). The I1 and I2 faults began to develop on both sides of the model at about the same time, depending on the type of experiment (Table 3). In most models with increased sedimentation, both faults appeared earlier, at ca. 55% of shortening (45–50 min), with respect to the experiments with less sedimentation (ca. 81% of shortening, and at 70–80 min) (Table 3). This coincided inversely with the delay in the initiation of the inversion with increased sedimentation mentioned above, without deformation on the surface of the sand-box during this period (Fig. 4g). It is possible that thrust faults were generated earlier and deeper than recorded and that they absorbed compressive deformation in this period, but we did not have access to this information because we did not scan the interior of the sandbox during the evolution of the experiment.

It is worth noting that surface analyses of the evolution of the experiments showed that the fault I2 was not developed only in models without sedimentation in both extension and compression. In this case, two thrust faults verging towards the piston were developed, an internal (i1) and an external fault (I1) (Fig. 5d). The internal fault i1 was developed shallowly in other experiments with low sedimentation and did not emerge at the surface (Fig. 5e and h). This is explained by the slight or complete absence of sedimentary load in the grabens and, therefore, the freedom to develop an internal fault. In the case of complete internal sedimentation in the grabens, in extension or compression, this structure did not develop (Fig. 5f, j, k, l and m).

In all cases, one of the new faults, I1 or I2, was rooted at the base of the silicone (Fig. 5d–m), and in some cases absorbed large amounts of shortening (Table 3 and Fig. 5f and j). It should be noted that these faults absorbed more shortening than the reactivated faults due to their lower dip-angle (30°–40° versus 63°–76°, respectively). In the case of increased sedimentation in one of the grabens, either G1 or G2, the new thrust fault associated with that side, I1 and I2, was developed as a footwall shortcut (Huyghe, 1992; McClay, 1995) from the graben bounding reactivated fault (Fig. 5f, h, i, j and m). This structure was developed on the opposite side of the fault rooted in the silicone (Fig. 5d–m). However, it was not possible to define precisely the critical load in grabens at which the shortcuts were developed. Furthermore, the experiment with the greatest burden, with full internal sedimentation in the extensional phase and internal–external sedimentation in the compressive phase, the shortcuts were developed at very shallow levels (Fig. 5m). This is explained by the greater load within the associated graben (G1) that prevented the development of the short-cuts at deeper levels. The shortcut faults absorbed only ca. 7% of the total shortening (1 mm/15 mm), and the bulk of the shortening in this experiment, ca. 40% (6 mm/15 mm), was absorbed by I1 on the opposite side (Table 3).

We observed that a gradual increase of sedimentation also involved a gradual decrease in the percentage of inversion on the previous normal faults (see percentages obtained from Eq. (1) recorded in Fig. 5d–m and Table 3). In the models performed without sedimentation in compression, the percentage of inversion varied from 80% in the case without sedimentation during the previous extension to only 47% with full sedimentation in extension (Fig. 5d–f and Table 3). In turn, in compression models performed without sedimentation during the extensional phase there was also a decrease in the percentage of inversion. Inversion varied from 80% in the case without sedimentation during compression to 70% in the case of full sedimentation during compression (Fig. 5d, g and i). We note here that the influence of sedimentation during the

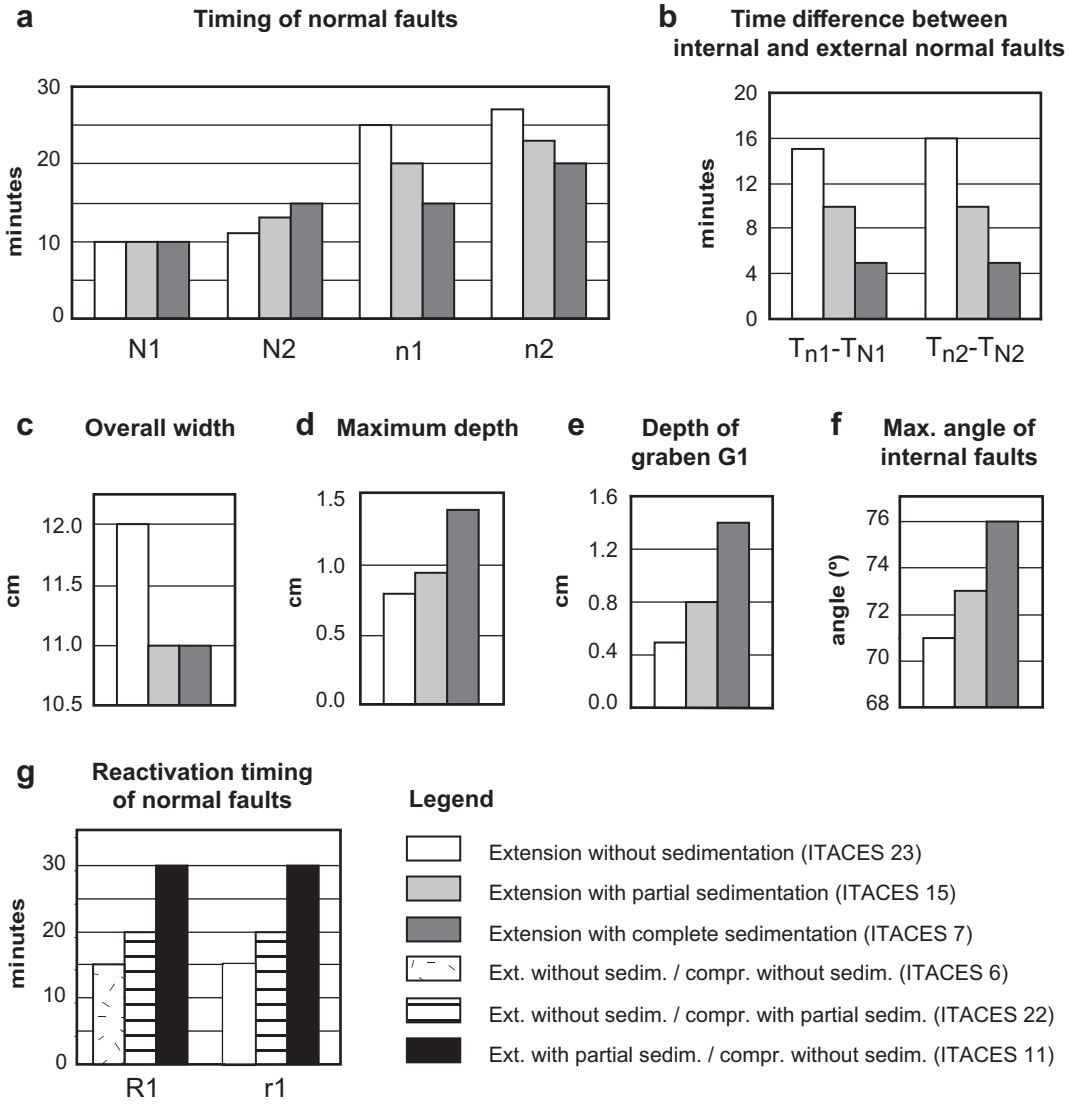

Fig. 4. Graphs representing the timing and the dimentions of the structural features formed during the experiments depending on the amount of sediment accumulated in the basin. In extension: (a) time of occurrence of normal structures; (b) time difference between internal and external structures; (c) width of the basin; (d) maximum depth or depocentre of the basin; (e) depth of graben G1; (f) maximum angle of internal faults. In compression: (g) time at which the reactivation of normal faults occurred (only the experiments where this parameter is observable on the surface of the sand-box are considered). N, n, normal faults; T, timing; R, r, reactivated faults; Sedim., sedimentation; Compr., compression; 1 and 2, order of occurrence. In the legend, 'ITACES' refers to experimental run.

extensional phase prior to compressive phase is particularly significant for the amount of inversion in the system. In the case of full internal and external sedimentation during compression (Fig. 5j), we obtained a higher percentage of inversion (53%) than when only internal sedimentation occurred in the compressive phase (47%) (Fig. 5f).

In two series of experiments there is an inverse relationship between uplift, which is quantified from the maximum vertical displacement associated with the new thrust-faults, and the percentage of inversion, which represents the amount of reactivation along the former normal faults (Table 3). The cases include series without sedimentation in the compressive phase (Fig. 5d–f) and the series with internal–external sedimentation (Fig. 5k–m), for which we obtained values of 80%, 73% and 47% of inversion and an altitude peak of 2, 3 and 6.5 mm, respectively (Table 3). Therefore, for these series with an increased sedimentation, a progressively smaller inversion of the previously normal structures and a higher uplift of the system is associated with the new thrust faults.

3.3. Analysis of experimental results

3.3.1. Extensional phase

The locations of the external-bounding normal faults (N1 and N2) of the grabens were determined from the silicone strip beneath the sand layers along the model; the faults were generated at the edges of the strip. The results of the extensional experiments clearly indicate that there is a change in the depth of the basin directly related to the amount and timing of sedimentation. On one hand, as the basin is composed of two sub-grabens, the region where sedimentation begins supports a greater sedimentary load is the deepest sub-graben. With continuous sedimentation the vertical stress on the hanging wall does not decrease during deformation, in relation to the movement on the fault, and the displacement is easier here compared to the region without sedimentation. For models with partial and complete sedimentation, N1 was the first fault generated. Therefore, in its associated block a higher burden is produced, it subsides faster and generates

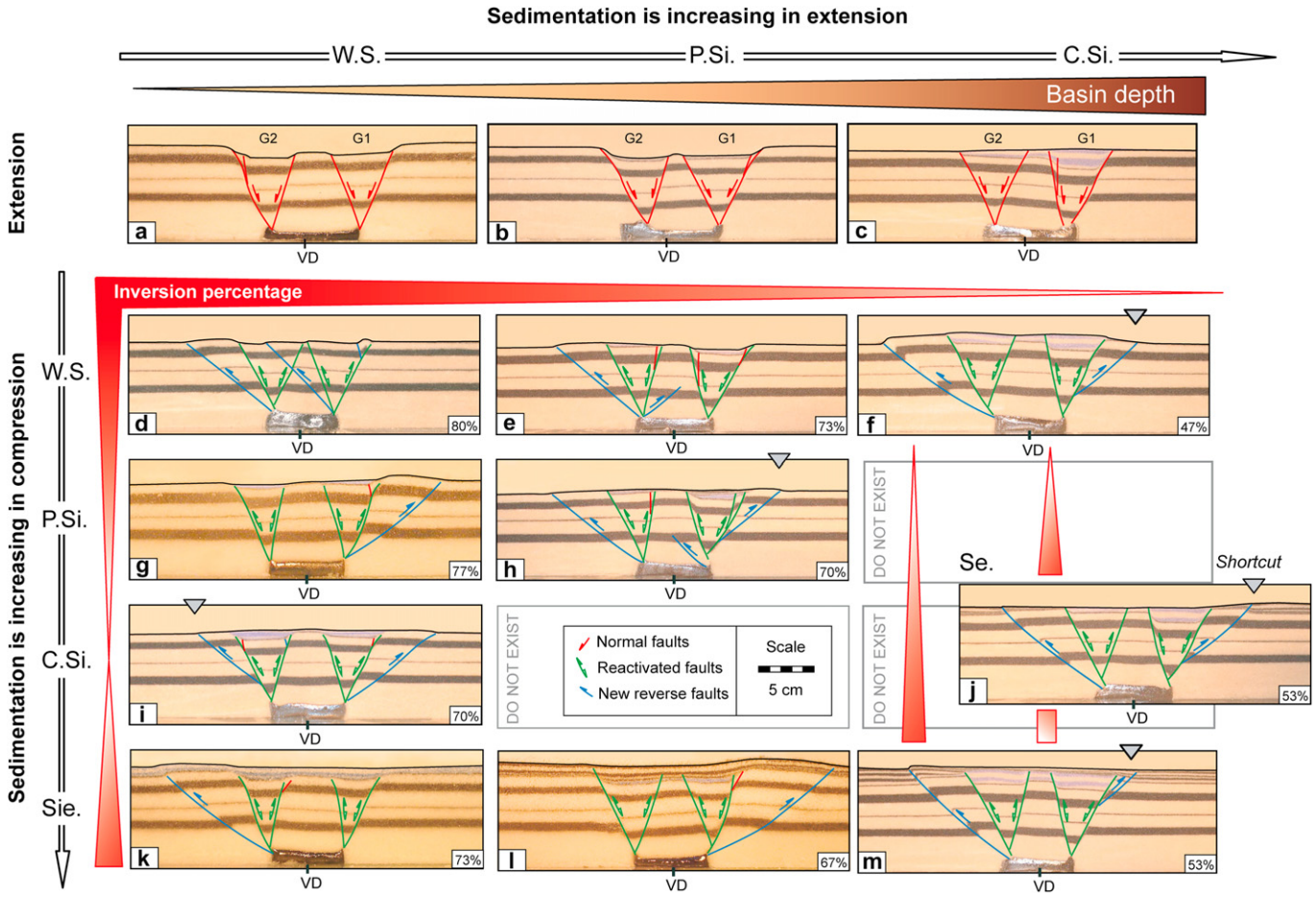

Fig. 5. (a–c) Figure summarizing the final features observed in the central sections of the extensional experiments with varying degrees of sedimentation (W.S., without sedimentation; P.Si., partial internal sedimentation; C.Si., complete internal sedimentation; Sie., internal and external sedimentation; Se., external sedimentation). The degraded top triangle (brown in color version) indicates the direction of subsidence of the basin in relation to the amount of sedimentation. (d–m) Summary of experiments in compression superimposed on extension. The horizontal direction indicates increase of sedimentation during the extension and the vertical direction indicates the increase of sedimentation during the compression. Each reactivated normal fault has a strike-slip component, which is not indicated for simplicity. The empty rectangles indicate 'not existing' cases (see the text for explanation). The grey horizontal degraded top triangle (red in digital version) indicates the progression rate of the inversion, the thicker and more intense color indicates a higher value, and the thin and low-intensity color indicates lower values. The small grey triangle on the top of some models indicates the location where the shortcut merges in the surface of the experiment. Reactivated faults are indicated with two arrowheads (green in digital version), and the new reverse faults are shown with one arrowhead (blue in digital version). The piston is located on the left side of the figure and the velocity discontinuity (VD) is indicated at the bottom. (For interpretation of the references to colour in this figure legend, the reader is referred to the web version of this article).

a depositional space where sediment is accumulated increasing the sedimentary load, i.e. G1 is generated. The descent of the block creates a larger local extension, which favors the formation of internal normal faults (n1 and n2), which are closer to N1. A higher sedimentary burden in G1 instigates the earlier development of the normal faults N1 and N2, accommodating the deformation associated with the subsident basin. Therefore, at a higher burden, N2 appears later and has a smaller displacement, probably because it is away from the area were the highest load is concentrated. This sequence of strain causes the basin to become asymmetrical. In this way, the higher movement observed from the faults N1 and n1 with respect to N2 and n2 is explained by an increased sedimentation. G1 is generated progressively earlier, supports the highest load, concentrates the deformation, and subsides faster in relation to G2.

Additionally, the gradual increase in dip-angle of the internal faults (n1, n2) in relation to the increased sedimentary load can be explained by the accommodation of a higher vertical displacement associated with the deepening of the basin with sedimentation.

3.3.2. *Shortening phase*

During the compressive phase the load caused by the sediments accumulated in the basin affects both the reactivation of normal faults and the generation of new reverse faults in such a way that with increased sedimentation within the basin there is a progressive decrease in the percentage of inversion. This is because the higher load of the sediments increases the vertical stress on the normal faults and makes their reactivation difficult. Also, the delay in the reactivation of normal faults to form reverse strike-slip faults, which depends on the increase of internal sedimentation in extension (Fig. 4g), is due to the increased difficulty of their reactivation due to the gradually increasing load.

Once the new faults are generated they begin to absorb most of the shortening, cushioning the process of tectonic inversion. A progressive increase in sedimentation allows the new inverse structures to appear earlier, which is mainly expressed in the larger displacement of I1 and/or I2 (e.g. Fig. 5f, j and m, see Table 3). The smaller amounts of inversion calculated for models with increased sedimentation are explained by the increased internal sedimentation in the grabens and thus by the great sediment load on the

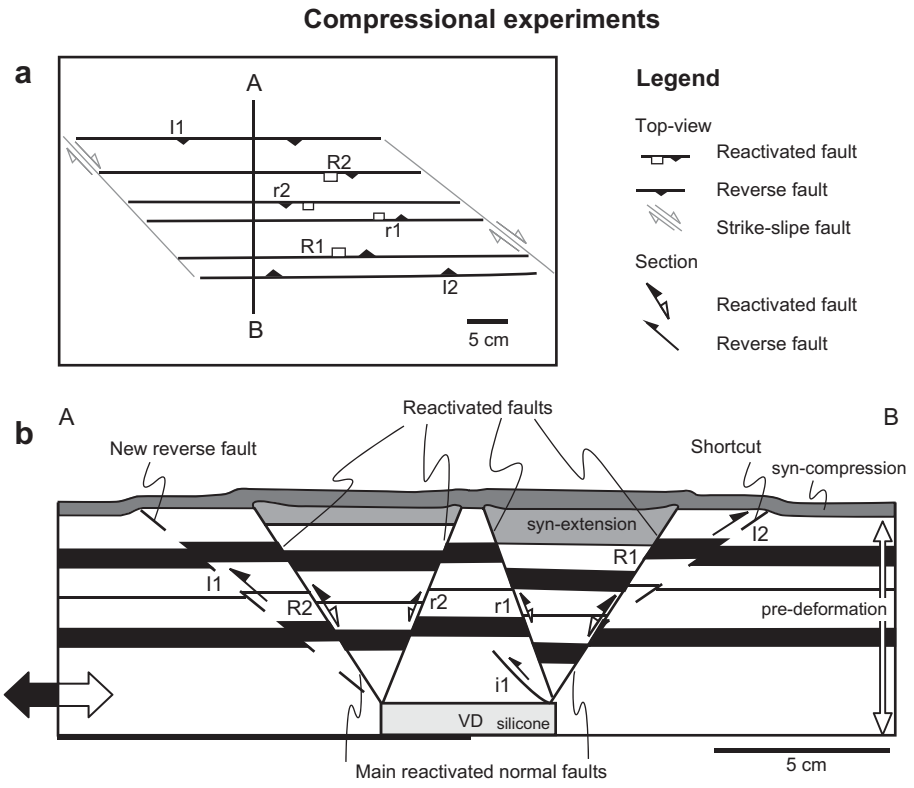

Fig. 6. Schematic illustration of the final state of the main structures generated with oblique compression experiments superimposed on the extensional experiments; we took a hypothetical extreme case, based on experiments 'f' and 'm' (Fig. 5), which include more model structural components. (a) Top-view from of the experiment. Boxes and triangles indicate the dip direction of the structures, normal and reverse respectively; faults with the two symbols refer to reactivated faults (compare with Fig. 2d–m). Strike-slip faults on the border of the models are also shown. The labeling of faults is as follows: R, r, reactivated faults; I, i, new reverse faults; 1 and 2, order of occurrence. (b) Section A–B through the central part of the experiment. 'A' corresponds to the mobile wall side, where the piston is located, and 'B' to the fixed wall side. This section represents a generic case of extension and compression with coeval sedimentation (syn-extension and syn-compressive, respectively). The geometry of the potential footwall shortcut that can be generated is indicated; arrows indicate the relative movement along the faults; VD indicates the velocity discontinuity under the silicone; grey areas indicate the location of potential accumulation of sediment in the syn-extensional and syn-compressive phases.

fault-plane of the basin bounding faults making their reactivation more difficult. In contrast, in the model with internal–external deposition (compare Fig. 5f vs. Fig. 5j and m) the additional burden on the outer edges tended to facilitate tectonic inversion despite the high internal load. Apparently, in this case, the relative difference of load has more affect than an absolute load within the basin. In addition, the external load occurs on the surface area where the trace of the thrust-fault should merge, therefore it is deduced that the burden represents an obstacle in the path of the fault that reduced its slip.

In areas with a lower load, the associated faults were rooted at the base of the silicone (Fig. 5d–m). This is may be because in this case the faults were able to uplift the entire sand column. In areas with higher burden it is more difficult for the faults to uplift the entire column. Therefore, it appears easier to produce displacement along only the lower part of the fault until a certain point, where it is possible to develop a shortcut (Fig. 5d–m). We defined distance "d" as the one between the top of the silicone and the lowest point of the footwall shortcut. In the experiments distance "d" increased with a higher sedimentary load (e.g. Fig. 5m), i.e. the shortcut became progressively more superficial.

The inverse relationship between uplift and the tectonic inversion in the two series of experiments is explained by the tectonic activity of the faults. Models with greater inversion are those where the movement along the fault-planes was greater, and thus the shortening absorbed by the new faults was smaller (Fig. 5d–m and Table 3). Therefore, the shortening is distributed in more faults and generates less uplift. In contrast, in experiments where the reactivation of faults is low (e.g. Fig. 5f and m) activity along the new faults is greater and shortening is concentrated in the two new faults that rise higher the entire system, with uplifts between 5.0 and 6.5 mm (Table 3). Similarly, with an increased internal load the inversion process along the previously formed normal faults is abandoned, new thrust faults are generated and have a greater total slip. This is reflected in an increase in the amount of absorbed shortening, as well as an increase in global uplift of the system. Therefore, a higher burden causes the new faults to absorb most of the contraccional deformation.

3.3.3. Global results

From the presented results it can be deduced that the inhibition of the inversion tectonic process caused by the sediment infill in the grabens is similar whether the load is applied during the extension phase or during the subsequent compressional phase. However, if the deposition occurs during the extensional phase the effect of load is more significant, because in that case compression starts with an extra weight within the grabens, and this weight increases during the rest of compressive phase. This decline in tectonic inversion depending on the increasing of sedimentation inside the basin is similar to what has been described in previous works (Nalpas and Brun, 1993; Nalpas, 1996; Brun and Nalpas, 1996; Dubois et al., 2002; Panien et al., 2005; Del Ventisette et al., 2006), where deposition was made contemporary to extension or between the period ending the extension and before the compression begins. These models have shown that in the absence of sedimentation in extensional-compressive models inversion

occurs along all normal faults, whereas with the addition of sediment the reactivation of the structures is limited (Dubois et al., 2002; Panien et al., 2005). Our results are consistent with these studies, but additionally show that there is a progression in the deformation style and amount of inversion with load addition, and also at which stage and location the load is applied.

One of the most interesting results derived from the performed experiments is the development of footwall shortcuts. These are generated in the region of higher load independently of the location of the silicone strip and the construction of the model. These are formed in the following manner: when the asymmetry of the basin exists, expressed as an increased sedimentation into one of the grabens, the new fault is developed as a shortcut rooted in the external reactivated fault. Apparently, this occurs because at a certain point along the inverted fault it is easier to transmit deformation to the sides developing a thrust fault. In general, the development of shortcuts occurs in cases where the sedimentation inside the grabens is complete, either during the extensional or the compressive phase. However, it was observed that for increasing sedimentation, for a same series of models, the newly formed thrust fault is generated more superficially. We propose that the increased sedimentation on a normal fault causes a greater displacement along the fault in the extensional phase. A greater slip will potentially be associated with a more curved fault-plane at the bottom of the device. This would help initiating the inversion in the bottom of the basin until shortcuts are generated.

4. Conclusive remarks

The results of our analogue experiments confirm the hypothesis that the sediment load is a major factor controlling the geometric evolution of an inverted extensional basin system:

- Furthermore, we showed that the load mainly controls the extent and timing of inverted faults. An increased sediment load causes a decrease in the tectonic inversion and the further development of thrust faults outside the basin.
- The reduction in tectonic inversion is relatively independent of whether the sedimentation occurs contemporaneously with the extension or compression. However, if sedimentation occurs during the first extensional phase the effect on the decline in tectonic inversion is more prominent.
- The new thrust faults can be developed in a region that has not been previously deformed, but if there is an asymmetry and increased sedimentation on the deeper side of the basin the new faults in that region can develop as shortcuts that are increasingly shallow with higher loads.
- Also, an accumulation of sediment on the outer edges of the basin facilitates the reactivation of normal faults and hampers the propagation of new thrust faults, as in this case the external load is applied in the region where the faults could emerge.

Acknowledgments

We acknowledge funding by the Departamento de Investigación y Desarrollo (DI), Universidad de Chile (Project 2004 DI, I2 04/02-2) to L. Pinto. Financial support for travel and stay in France for conducting analogue experiments given by the Bourse Amérique Latine at the Université Paul Sabatier (Toulouse III, France), French Institute of Research Collaboration (IRD), the ECOS-Chile Project C05U04 to T. Nalpas and V. Maksaev, the Facultad de Ciencias Físicas y Matemáticas of the Universidad de Chile, and the Analogue Modelling Laboratory at the Université de Rennes I (Rennes Géosciences). This research was also supported by the Fondecyt Project No. 1030965 and the Proyecto Anillo ACT N° 18 (Bicentenario-CONICYT), both awarded to R. Charrier. Careful reviews by Chiara Del Ventisette (Università degli Studi di Firenze) and Janine Kavanagh (University of Bristol) helped greatly to improve the manuscript. Discussions with Joseph Martinod (LMTG, Université Paul Sabatier), Mario Pardo (Universidad de Chile) and Lisandro Rojas (Sipetrol-ENAP, Chile) contributed significantly to the improvement of this article.

References

Allemand, P., Brun, J.P., 1991. Width of continental rifts and rheological layering of the lithosphere. Tectonophysics 188 (1–2), 63–69.
Allemand, P., Brun, J.P., Davy, P., Van Den Driessche, J., 1989. Symétrie et asymétrie des rifts et mécanismes d'amincissement de la lithosphère. B. Soc. Géol. Fr. 3, 445–451.
Balé, P., 1986. Tectonique caddomienne en Bretagne nord. Interaction décrochement chevauchement: champs de déformation et modélisations experimentales. Ph. D. thesis, Université de Rennes I, 361 pp.
Ballard, J.F., 1989. Approche géologique et mécanique des décollements dans la croûte supérieure. Ph.D. thesis, Université de Rennes I, 299 pp.
Bally, A.W., 1984. Tectogenèse et sismique réflexion. B. Soc. Géol. Fr. 26, 279–285.
Brun, J.P., Sokoutis, D., Van Den Driessche, J., 1994. Analogue modeling of detachment fault systems and core complexes. Geology 22, 319–322.
Brun, J.P., Nalpas, T., 1996. Graben inversion in nature and experiments. Tectonics 15 (3), 677–687.
Buchanan, J.G., Buchanan, P.G., 1995. Basin inversion. In: London, Special Publication 88. Geological Society, 596 pp.
Buchanan, P.G., McClay, K.R., 1991. Sandbox experiments of invertid listric and planar fault systems. Tectonophysics 188, 97–115.
Buchanan, P., McClay, K.R., 1992. Experiments on basin inversion above reactived domino fault. Mar. Petrol. Geol. 9, 486–500.
Burns, W.M., Jordan, T.E., 1999. Extension in the Southern Andes as evidenced by an Oligo-Miocene age intra-arc basin. In: IV International Symposium on Andean Geodynamics (ISAG). IRD, Göttingen, Germany, pp. 115–118.
Charrier, R., Wyss, A.R., Flynn, J.J., Swisher III, C.C., Spichiger, S., Zapatta, F., 1994. Nuevos antecedentes estratigráficos y estructurales para las Formaciones Coya-Machalí y Abanico, entre 33° 50′ y 35°. In: Cordillera Principal Chilena. VII Congreso Geológico Chileno, vol. 2. Concepción. 1316–1319.
Charrier, R., Baeza, O., Elgueta, S., Flynn, J.J., Gans, P., Kay, S.M., Muñoz, N., Wyss, A.R., Zurita, E., 2002. Evidence for Cenozoic extensional basin development and tectonic inversion south of the flat-slab segment, southern Central Andes, Chile (33°–36°S.L.). J.S. Am. Earth Sci. 15, 117–139.
Charrier, R., Bustamante, M., Comte, D., Elgueta, S., Flynn, J.J., Iturra, N., Muñoz, N., Pardo, M., Thiele, R., Wyss, A.R., 2005. The Abanico extensional basin: regional extension, chronology of tectonic inversion and relation to shallow seismic activity and Andean uplift. N. Jb. Geol. Palaont. Abh. 236, 43–77.
Charrier, R., Pinto, L., Rodríguez, M., 2007. The geology of Chile. Chapter 3. In: Gibbonds, W., Moreno, T. (Eds.), Tectonostratigraphic Evolution of the Andean Orogen in Chile. Special Publications, UK. The Geological Society, London, pp. 21–116.
Cooper, M.A., Williams, G.D., 1989. Inversion tectonics. In: Special Publication 44. Geological Society, London, pp. 17–39.
Corti, G., Bonini, M., Conticelli, S., Innocenti, F., Manetti, P., Sokoutis, D., 2003. Analogue modelling of continental extension: a review focused on the relations between the patterns of deformation and the presence of magma. Earth-Sci. Rev. 63, 169–247.
Davy, P., Cobbold, P.R., 1991. Experiments on shortening of a 4-layer model of the continental lithosphere. Tectonophysics 188, 1–25.
Del Ventisette, Ch., Montanari, D., Bonini, M., Sani, F., 2005. Positive fault inversion triggering "intrusive diapirism": an analogue modelling perspective. Terra Nova 17 (5), 478–485.
Del Ventisette, Ch., Montarani, D., Sani, F., Bonini, M., 2006. Basin inversion and fault reactivation in laboratory experiments. In: Tavarnelli, E., Butler, R., Grasso, M. (Eds.), Tectonic Inversion Processes and Structural Inheritance in Mountain Belts. J. Struct. Geol. 28 (11), 2067–2083. doi:10.1016/j.jsg.2006.07.012.
Dubois, A., Odonne, F., Massonnat, G., Lebourg, T., Fabre, R., 2002. Analogue modeling of fault reactivation: tectonic inversion and oblique remobilisation of grabens. J. Struct. Geol. 24, 1741–1752.
Faugère, F., Brun, J.P., 1984. Modelisation experimentale de la distention continentale. C.R. Acad. Sci. II 299, 365–370.
Fock, A., 2005. Cronología y tectónica de la exhumación en el Neógeno de los Andes de Chile central entre los 33° y los 34°S. Master Thesis, Departamento de Geología, Universidad de Chile, 179 pp.
Fock, A., Charrier, R., Farías, M., Muñoz, M., 2006a. Fallas de vergencia oeste en la Cordillera Principal de Chile Central: Inversión de la cuenca de Abanico (33°–34°S). Revista de la Asociación Geológica Argentina, Publicación Especial 6, 48–55.
Fock, A., Charrier, R., Maksaev, V., Farías, M., Álvarez, P., 2006b. Evolución cenozoica de los Andes de Chile Central (33°–34°S). XI Congreso Geológico Chileno vol II, 205–208.

Garrido, I., Riveros, M., Cladouhos, T., Espiñeira, D., Allmendinger, R., 1994. Modelo geológico estructural yacimiento El Teniente. VII Congreso Geológico Chileno. Concepción 2, 1553–1558.
Garrido, I., Cembrano, J., Siña, A., Stedman, P., Yáñez, G., 2002. High magma oxidation state and bulk crustal shortening: key factors in the genesis of Andean porphyry copper deposits, central Chile (31–34°S). Rev. Geol. Chile 29 (1), 43–54.
Gartrell, A., Hudson, C., Evans, B., 2005. The influence of basement faults during extension and oblique inversion of the Makassar Straits rift system: insights from analog models. AAPG Bull. 89 (4), 495–506. doi:10.1306/12010404018.
Godoy, E., 2005. High magma oxidation state and bulk crustal shortening: key factors in the genesis of Andean porphyry copper deposits, central Chile (31–34°S). Rev. Geol. Chile 32 (1), 155–157.
Godoy, E., Lara, L., 1994. Segmentación estructural andina a los 33°–34°: nuevos datos en la Cordillera Principal. VII Congreso Geológico Chileno. Concepción 2, 1344–1348.
Godoy, E., Yáñez, G., Vera, E., 1999. Inversion of an Oligocene volcano-tectonic basin and uplifting of its superimposed Miocene magmatic arc in the Central Chilean Andes: first seismic and gravity evidences. Tectonophysics 306 (2), 217–236.
Hansen, W.R., 1986. Neogene tectonics and geomorphology of the eastern Uinta Mountains in Utah, Colorado and Wyoming. United States Geological Survey, Professional Paper 1356, 78 pp.
Huyghe, P., 1992. Enregistrement sédimentaire des déformations intraplaques: l'exemple de l'inversion structurale d'un bassin de la Mer du Nord. Ph.D. thesis, Université Joseph Fourier - Grenoble I, 258 pp.
Jordan, T.E., Burns, W.M., Veiga, R., Pángaro, F., Copeland, P., Kelley, S., Mpodozis, C., 2001. Extension and basin formation in the Southern Andes caused by increased convergence rate: a mid-Cenozoic trigger for the Andes. Tectonics 20 (3), 308–324.
Kay, S.M., Kurtz, A., 1995. Magmatic and Tectonic Characterization of the El Teniente Region. Informe, CODELCO, Chile, 180 pp.
Keep, M., McClay, K.R., 1997. Analogue modelling of multiphase rift systems. Tectonophysics 273, 239–270.
Knott, S.D., Beach, A., Welbon, A.I., Brockbank, P.J., 1995. Basin inversion in the Gulf of Suez: implications for exploration and development in failed rifts. In: Buchanan, J.G., Buchanan, P.G. (Eds.), Basin Inversion. Special Publication 88. Geological Society, London, pp. 59–81.
Koopman, A., Speksnijder, A., Horsfield, W.T., 1987. Sandbox model studies of inversion tectonics. Tectonophysics 137, 379–388.
Lamplugh, G.W., 1920. The structure of the Weald and analogous tracts. Quart. J. Geol. Soc. London 15, LXXIII–XCV.
Letouzey, J., 1990. Fault reactivation, inversion and fold-thrust belt. In: Letouzey, J. (Ed.), Petroleum and Tectonic in Mobile Belts. Technip, Paris, pp. 101–128.
Lowell, J.D., 1995. Mechanics of basin inversion from worldwide examples. In: Buchanan, J.G., Buchanan, P.G. (Eds.), Basin Inversion. Special Publication 88. Geological Society, London, pp. 39–57.
Malavielle, J., 1984. Modélisation expérimentale des chevauchements imbriqués: application aux chaînes de montagnes. B. Soc. Géol. Fr 7, 129–138.
McClay, K.R., 1989. Analogue models of inversion tectonics. In: Cooper, M.A., Williams, G.D. (Eds.), Inversion Tectonics. Special Publication 44. Geological Society, London, pp. 41–59.
McClay, K.R., 1995. The geometries and kinematic of inverted fault systems: a review of analogue model studies. In: Buchanan, J.G., Buchanan, P.G. (Eds.), Basin Inversion. Special Publication 88. Geological Society, London, pp. 97–118.
McClay, K.R., White, M.J., 1995. Analogue modelling of orthogonal and oblique rifting. Mar. Petrol. Geol. 12 (2), 137–151.
Mitra, S., 1993. Geometry and kinematic evolution of inversion structures. Am. Assoc. Petr. Geol. B 77 (7), 1159–1191.
Muñoz, C., Pinto, L., Nalpas, T., 7–11 Agosto 2006. Análisis de la influencia de la sedimentación tectónica por medio de modelación analógica. XI Congreso Geológico Chileno, Antofagasta.
Nalpas, T., 1996. Inversion des grabens du Sud de la Mer du Nord. Données de subsurface et modélisation analogique. Ph.D. thesis, Géosciences Rennes, Université de Rennes, France, 245 pp. ISBN: 2-905532-70-X.
Nalpas, T., Brun, J.P., 1993. Salt flow and diapirism related to extension at crustal scale. Tectonophysics 228, 349–362.
Nalpas, T., Le Douaran, S., Brun, J.P., Unternehr, P., Richert, J.P., 1995. Inversion of the Broad Fourteens Basin (offshore Netherlands), a small scale model investigation. Sedimentary Geology 95, 237–250.
Nyström, J., Parada, M., Vergara, M., 1993. Sr–Nd isotope compositions of Cretaceous to Miocene volcanic rocks in Central Chile: a trend towards a MORB signature and a reversal with time. II International Symposium on Andean Geodynamics (ISAG), Oxford, UK, IRD, pp. 411–414.
Nyström, J.O., Vergara, M., Morata, D., Levi, B., 2003. Tertiary volcanism during extension in the Andean foothills of central Chile (33°15′–33°45′S). Geol. Soc. Am. Bull. 115, 1523–1537.
Panien, M., Schreurs, G., Pfiffner, A., 2005. Sandbox experiments on basin inversion: testing the influence of basin orientation and basin fill. J. Struct. Geol. 27, 433–445.
Pardo-Casas, F., Molnar, P., 1987. Relative motion of the Nazca (Farallon) and South American plates since Late Cretaceous time. Tectonics 6, 233–248.
Pruvost, P., 1930. Sedimentation et subsidence. Centenaire de la Société Géologique de France. Livre Jubilaire 1830–1930. Tome II, Paris, 443 pp.
Richard, P.D., Cobbold, P.R., 1990. Experimental insights into partitioning of fault motions in continental convergent wrench zones. Annales Tectonicae, Special Issue 4, 35–44.
Rivera, O., Cembrano, J., 2000. Modelo de formación de cuencas volcano-tectónicas en zonas de transferencia oblicuas a la cadena andina: el caso de las cuencas oligo-miocénicas de Chile central y su relación con estructuras NWW-NW (33°00′–34°30′S). IX Congreso Geológico Chileno, Puerto Varas, vol. 2, pp. 631–636.
Rivera, O., Falcón, F., 2000. Secuencias de relleno de cuencas volcano-tectónicas transversales oligo-miocenas en los alrededores del yacimiento El Teniente (33°45′–34°30′). IX Congreso Geológico Chileno, Puerto Varas, vol. 1, pp. 819–823.
Stille, H., 1924. Grundfragen der vergleichenden Tektonik. Gebrüder Borntraeger, Berlin, 443 pp.
Stone, D.S., 5 October 1989. Uinta Mountains: An Inverted Proterozoic Aulacogen. Rocky Mountain Association Geologists Outcrop.
Tron, V., Brun, J.P., 1991. Experiments on oblique rifting in brittle–ductile systems. Tectonophysics 188, 71–84.
Vendeville, B., Cobbold, P.R., Davy, P., Brun, J.P., Choukroune, P., 1987. Physical models of extensional tectonics at various scales. In: Coward, M.P., Dewey, J.F., Hancock, P.L. (Eds.), Continental Extensional Tectonics. Geological Society Special Publication 28, pp. 95–107.
Vergara, M., Drake, R., 1979. Edades K/Ar en secuencias volcánicas continentales postneocomianas de Chile central: Su depositación en cuencas intermontanas restringidas. Revista de la Asociación Geológica Argentina 34, 42–52.
Voigt, E., 1963. Uber Randtroge vor Scholtenrandern und ihre Bedeutung im Gebiet mit der Mitteleuropaischen Senke und angrenzender Gebiete. Zeitschrift der Deutschen Geologischen Gesellschaft 114, 378–418.
Walker, I.M., Cooper, W.G., 1986. The structural and stratigraphy evolution of the N. E. margin of the sole Pit basin. In: Brooks, J., Glennie, K. (Eds.), Petroleum Geology of Northwest Europe. Graham and Trotman, London, pp. 263–275.
Yamada, Y., McClay, K.R., 2003a. Application of geometric models to inverted listric fault systems in sandbox experiments. Paper 1: 2D hanging wall deformation and section restoration. J. Struct. Geol. 25, 1551–1560.
Yamada, Y., McClay, K.R., 2003b. Application of geometric models to inverted listric fault systems in sandbox experiments. Paper 2: insights for possible along strike migration of material during 3D hanging wall deformation. J. Struct. Geol. 25, 1331–1336.